

AD-A056 297

NAVAL POSTGRADUATE SCHOOL MONTEREY CALIF
MORPHOLOGICAL EVIDENCE FOR A PITTING MECHANISM IN DILUTE ALUMIN--ETC(U)
JUN 78 J PERKINS, J R CUMMINGS, K J GRAHAM

F/G 11/6

UNCLASSIFIED

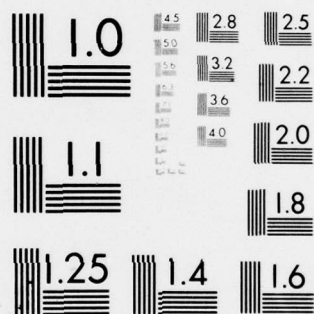
NPS-69PS-78-005

NL

| OF |

AD
A056297





MICROCOPY RESOLUTION TEST CHART
NATIONAL BUREAU OF STANDARDS-1963-A

AD A 056297

AD No. _____
DDC FILE COPY

LEVEL *II*

2

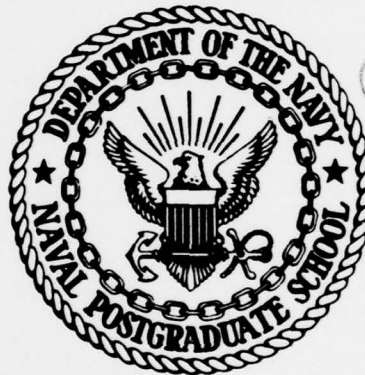
14 NPS-69PS-78-005, NPS-TR-9

NAVAL POSTGRADUATE SCHOOL

Monterey, California

16 RR02248

17 RR0220801



DDC
RECEIVED
JUL 17 1978
Jc F

9 Interim rept. Mar-Jun 78,

6 MORPHOLOGICAL EVIDENCE FOR A PITTING MECHANISM IN DILUTE ALUMINUM ALLOYS.

by

10 J. Perkins, J. R. Cummings and K. J. Graham

11 June 1978

12 18p.

Technical Report No. 9
To the Office of Naval Research
Contract No. N00014-78-WR-80105
NR-036-120

Approved for public release; distribution unlimited.
Reproduction in whole or in part is permitted for any purpose of the
United States Government.

78 07 10 126

NAVAL POSTGRADUATE SCHOOL
Monterey, California

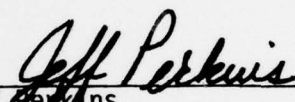
Rear Admiral T. R. Dedman
Superintendent

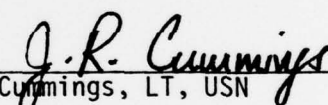
Jack R. Borsting
Provost

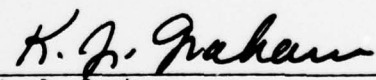
The work reported herein was supported by the Office of Naval Research,
Naval Ship Systems Command, Metallurgy Program Office, Code 471, Arlington,
VA, 22217, through Contract No. N00014-78-WR-80105, NR-036-120.

Reproduction of all or part of this report is authorized.

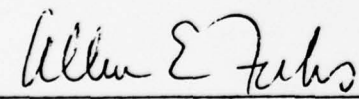
This report was prepared by:

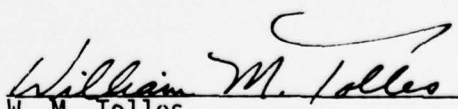

Jeff Perkins
Associate Professor of Materials Science


J. R. Cummings, LT, USN


K. J. Graham
Research Chemist
Materials Science and Chemistry Group

Reviewed by:


Allen E. Fuhs, Chairman
Department of Mechanical Engineering


W. M. Tolles
Dean of Research, Acting

UNCLASSIFIED

SECURITY CLASSIFICATION OF THIS PAGE (When Data Entered)

REPORT DOCUMENTATION PAGE		READ INSTRUCTIONS BEFORE COMPLETING FORM
1. REPORT NUMBER NPS-69PS-78-005	2. GOVT ACCESSION NO.	3. RECIPIENT'S CATALOG NUMBER
4. TITLE (and Subtitle) MORPHOLOGICAL EVIDENCE FOR A PITTING MECHANISM IN DILUTE ALUMINUM ALLOYS		5. TYPE OF REPORT & PERIOD COVERED Interim, 3/78 to 6/78
		6. PERFORMING ORG. REPORT NUMBER Technical Report No. 9
7. AUTHOR(s) J. PERKINS, J. R. CUMMINGS AND K. J. GRAHAM		8. CONTRACT OR GRANT NUMBER(s) N00014-78-WR-80105, NR-036-120
9. PERFORMING ORGANIZATION NAME AND ADDRESS Materials Science and Chemistry Group, Dept. of Mechanical Engineering, Naval Postgraduate School, Monterey, CA 93940		10. PROGRAM ELEMENT, PROJECT, TASK AREA & WORK UNIT NUMBERS Program Element: 61153N Project: RR022-08-01
11. CONTROLLING OFFICE NAME AND ADDRESS Office of Naval Research, Metallurgy Program Office, Code 471, Arlington, VA 22217		12. REPORT DATE June 1978
		13. NUMBER OF PAGES
14. MONITORING AGENCY NAME & ADDRESS (if different from Controlling Office)		15. SECURITY CLASS. (of this report) UNCLASSIFIED
		15a. DECLASSIFICATION/DOWNGRADING SCHEDULE
16. DISTRIBUTION STATEMENT (of this Report) Approved for public release; distribution unlimited. Reproduction in whole or in part is permitted for any purpose of the United States Government.		
17. DISTRIBUTION STATEMENT (of the abstract entered in Block 20, if different from Report)		
18. SUPPLEMENTARY NOTES		
19. KEY WORDS (Continue on reverse side if necessary and identify by block number) pitting, aluminum alloys, corrosion products, scanning electron microscopy.		
20. ABSTRACT (Continue on reverse side if necessary and identify by block number) In the course of an investigation of the seawater corrosion behavior of several dilute aluminum alloys, direct microscopic evidence of pitting phenomena was obtained. Observations, obtained by scanning electron microscopy after gal- vanic corrosion exposures, illustrate a pitting mechanism involving the extrusion of columns of corrosion product from pits by the action of hydrogen gas generated inside the pits. The macroscopic dissolution patterns of the various alloys and their respective microscopic dissolution morphologies		

DD FORM 1473
1 JAN 73EDITION OF 1 NOV 65 IS OBSOLETE
S/N 0102-014-6601

UNCLASSIFIED

SECURITY CLASSIFICATION OF THIS PAGE (When Data Entered)

78 07 10 126

UNCLASSIFIED

SECURITY CLASSIFICATION OF THIS PAGE(When Data Entered)

20. are also described. The observations support the classical model for pitting of aluminum originally presented by Edeleanu and Evans.

ACCESSION FOR	
NTIS	White Section <input checked="" type="checkbox"/>
DDC	Buff Section <input type="checkbox"/>
UNANNOUNCED	<input type="checkbox"/>
JUSTIFICATION	
BY	
DISTRIBUTION AVAILABILITY CODES	
Do	SPECIAL
A	

UNCLASSIFIED

SECURITY CLASSIFICATION OF THIS PAGE(When Data Entered)

MORPHOLOGICAL EVIDENCE FOR A PITTING MECHANISM IN DILUTE ALUMINUM ALLOYS

J. Perkins, J. R. Cummings, and K. J. Graham

Materials Science and Chemistry Group, Code 61Ps

Naval Postgraduate School, Monterey, CA 93940

In the course of a recent investigation (1) of the saltwater corrosion behavior of several dilute aluminum alloys, some dramatic direct microscopic evidence of pitting phenomena was obtained. Observations, obtained by scanning electron microscopy after galvanic corrosion exposures, illustrate a pitting mechanism involving the extrusion of columns of corrosion product from pits by the action of hydrogen gas generated inside the pits. Because this behavior does not relate directly to the goals of the original study of these alloys (1), it is being reported separately in this note.

The alloys investigated were several dilute aluminum alloys designed especially for application as sacrificial anodes in marine cathodic protection systems. The nominal compositions of the alloys discussed in this note are given in Table I. These alloys were exposed in natural galvanic couples (area ratio 1:27) with steel in aerated synthetic seawater; the experimental details have been presented in an earlier report (1). Under these conditions, the aluminum alloys (which were monitored for galvanic current and potential) operated with a steady-state anodic current density of about 0.8 mA/cm^2 and the anodic polarization of the alloys was to about -1.0V (vs.SCE); (the corrosion potentials of the three alloys G, R, and K were measured (1) as -1.35 , -1.15 , and -1.2V , all vs.SCE, respectively).

Macroscopic Dissolution Behavior

Each of the dilute aluminum alloys has its own unique pattern of dissolution on the macroscopic scale. Alloy G tends to initiate large dissolution cavities along the machined edges and corners of samples (Figure 1a), Alloy R forms vertically aligned elongated dissolution cavities on the broad faces (Figure 1b), and Alloy K tends to exhibit profuse pitting (1c). These behaviors have been discussed in an earlier report (1) and will not be considered in detail here. The active regions of the anodes are confined to the

dissolution regions; the rest of the surface is covered with a thin compact film. All of the alloys tend to rapidly form (within a few hours) a certain distribution of initial dissolution sites, which then slowly expand laterally, as opposed to initiation of more sites.

The dissolution surfaces of Alloys G and R accumulate little if any corrosion product in the early stages of attack (first 50 hours) while Alloy K shows distinctly more accumulation than the other alloys, with about as much product after 1 hour as the others show in 50 hours (1). Only after the dissolution surfaces become somewhat filmed-over with corrosion product do the fine (micron scale) pits discussed in this paper appear; i.e., these fine pits are not an initial phenomena, and are distinguished from the larger initial dissolution cavities. The samples, exposed in galvanic couples, initially experience a relatively high current density (about 4 to 8 mA/cm²) which then falls off to a stable level of about 0.8 mA/cm² (1); this decrease corresponds mainly to the accumulation of calcareous deposits on the surfaces of the companion cathodes (steel); this reduces the galvanic current, and when the current falls, and the aluminum anodes are less active, they tend to develop corrosion product films over their dissolution regions (1). When this occurs, the conditions are apparently established for true pitting phenomena, i.e., occluded cells are established, and attack accelerates perpendicular to the surface, forming deep pin-hole cavities.

Microscopic Dissolution Behavior

When the dissolution surfaces of these alloys are examined at high magnification in the scanning electron microscope, each alloy is seen to have its own characteristic dissolution morphology. In each case, the attack is distinctly crystallographic in nature, but the specific form differs for each alloy, as illustrated in Figure 2. Alloy G exhibits a unique step pattern, with very little corrosion product accumulation (Figure 2a). Alloy R develops a distinctly different dissolution morphology, consisting of an array of sharp crystallographic peaks (Figure 2b) and in this case also there is little corrosion product on the reacting areas of the surface. Alloy K shows a much less distinct etching pattern than the other alloys, and there is a tendency to accumulate more corrosion product, so that the underlying dissolution morphology is only seen when the corrosion product is knocked off the surface; a tendency to intergranular penetration is also seen for Alloy K. Of course,

because the alloys are exhibiting crystallographic etching, the exact appearance of the dissolution pattern varies with grain orientation (1).

Microscopic Observations of a Pitting Mechanism

After about 50 hours galvanic exposure, Alloys G and R begin to develop a discontinuous film over their dissolution surfaces. When this occurs, evidence of a true pitting phenomenon begins to be seen. Mushroom-like mounds of corrosion product begin to push their way up at certain sites in the film (Figure 3a). These emerging forms characteristically have a smooth hemispherical cap, and by their form appear to be discontinuously extruded from within the underlying pits (Figure 3b). These eruptions are nearly always located within the mud-cracked film over the dissolution regions; only occasionally are such forms seen to emerge on the unattacked areas of the surface (Figures 4a, 4b). These forms are assumed to consist of a hydrated aluminum oxide corrosion product which has been emitted from the pit mouths by the action of hydrogen gas pressure built up within the occluded cells (pits).

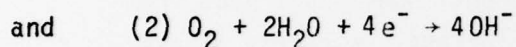
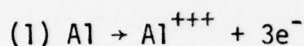
Alloy K shows a somewhat different morphological manifestation of fine-scale pitting phenomenon, consisting of arrays of perfectly hemispherical hollow domes located on the unattacked surface areas of the anode (Figure 3c). These appear much earlier in the exposure history of the anode than the extruded forms on Alloys G and R. These forms again appear to be the result of hydrogen gas evolution within underlying pits. In this case, the pressure inflates the domes by deformation of the general film material. These domes are known to be thin hollow shells because they often are observed broken open (Figure 5), probably due to handling of the specimens. Even when the surface is studied at high magnification, these domes cannot be clearly associated with any physical feature in the general film structure, such as cracks; note in Figure 3c that the general film reflects the underlying grinding marks on the specimen. When these hemispherical pods crack open, an interior filament of very white corrosion product can be seen (Figure 5).

Discussion

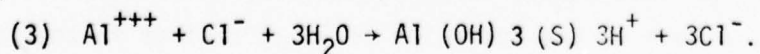
Aluminum is well-known to pit in chloride-containing aqueous solutions, including seawater (2-6). In this study, the initiation of dissolution is accomplished in all three alloys by the formation of local regions in the surface film. These dissolution regions tend to spread laterally over the surface

more rapidly than they penetrate, the anodic and cathodic reactions are not separated, and occluded cells are not formed; thus, this behavior is not based on a classical pitting mechanism. However, later in the history of the samples, when the dissolution regions become somewhat filmed over with corrosion product, true pitting phenomena is exhibited, with separated anodic and cathodic reaction sites, occluded cells, and accelerated penetration perpendicular to the surface.

In a solution such as seawater, the natural anodic and cathodic half-cell reactions on aluminum may be considered to be

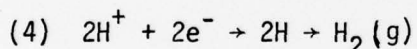


respectively. Without considering the exact mechanism by which the true pits initiate, which is historically a controversial matter (7-11), we may assume that when the pits initiate these half-cell reactions become physically separated, with the aluminum dissolution reaction occurring within the pit site, and the oxygen reduction reaction occurring outside of it, on the surrounding, film-covered surface (2). In the case of the samples in the present study, which were anodically polarized to some extent due to coupling with steel samples, the oxygen cathodic half-cell reaction may not occur at all on the aluminum surface, but rather on the steel cathode in the galvanic couple; this does not affect the argument that follows whatsoever. Typically, a high cathode-to-anode surface area ratio is set up once the pitting situation is created, so that a high local anodic current density is created in the pit sites. Also, because there is limited access of O_2 to the pit interior, the O_2 concentration in the pit solution (the anolyte) rapidly becomes nil (2). The generally accepted theories for pitting (2) then argue that due to the resultant local buildup of positive charge due to metal ion concentration within the pit, migration of anions from the bulk solution is encouraged to maintain charge balance, and that particularly the mobile Cl^- ion, if present, will be attracted to the pit interior. Of course in seawater, there is an available supply of Cl^- ions, and it is considered that when the anolyte composition becomes sufficiently concentrated in Al^{+++} and Cl^- , a hydrolysis (water breakdown) reaction occurs (2). This may be represented by a reaction such as:



Note that this reaction creates a solid corrosion product and lowers the pH within the pit, while maintaining the chloride ion concentration. Since both the low pH and high Cl^- ion concentration tend to facilitate the anodic dissolution reaction, the overall process tends to accelerate; this is sometimes referred to as autocatalytic behavior (2). In most models of the pitting process, formation of the solid corrosion product is assumed to occur at the mouth of the pit, as a membrane or mound (3), which serves to further isolate the pit solution (anolyte) from the bulk solution; the occluded cell situation is enhanced. In the present study we are able to see directly the enhanced local generation of solid corrosion product at the pit sites. We see both solid mounds (Alloys G and R) and thin membranes (Alloy K) over pit entrances in the alloys discussed in this paper. It is also evident here that the solid corrosion products precipitate in such a way as to effectively seal the pit mouth, to the extent that hydrogen gas generation within the pit can build up pressure and physically move or deform the mound.

It is well known that the anolyte composition changes considerably during pit propagation (2), with a large decrease in pH and simultaneous increase in aggressive anion concentration. It is also well accepted that in this acidic occluded cell, reduction of hydrogen ions will occur, according to the reaction



creating hydrogen gas (4). Even in single metal situations, it is known that this reaction of H_2 evolution within pits plays an important role in supporting the anodic dissolution reaction, and under conditions of increased anodic polarization, H_2 gas evolution from within pits is quite evident (3). The classic study of Edeleanu and Evans (2) included direct observation that (hydrogen) gas bubbles come from within pits in the anodic attack of aluminum. With the present microscopic observations we are able to directly confirm the existence of a continuous formation process for the solid corrosion product of equation (3), as well as observe its morphology, and from the morphological observations we are able, by strong inference, to support the concept of hydrogen gas evolution within pits represented by equation (4). The gas is evolved within a sealed cell, and builds up pressure that may be released periodically by extruding the solid corrosion product out of the pit mouth, or which may act continuously to form inflated hemispherical shells over the pit

opening. Further study is required to determine the factors which cause these different morphological manifestations of the basic pitting reactions. Certainly, variations in the base alloy composition and consequent variations in the character of the surface films are likely to have important influences.

Acknowledgement

This work was supported by the Office of Naval Research through contract N00014-78-WR-80105, NR-036-120.

REFERENCES

1. J. Perkins, J. R. Cummings, R. A. Reinhardt, and K. J. Graham, "Corrosion Behavior of Aluminum Alloys Intended for Sacrificial Anode Applications in Seawater," NPS-69PS-78-002, Technical Report No. 6 prepared for the Office of Naval Research, Contract N00014-78-WR-80105, NR-036-120, March 1978.
2. C. Edeleanu and U. R. Evans, "The Causes of the Localized Character of Corrosion on Aluminum," Trans. Faraday Soc. 47, 1121 (1951).
3. J. A. Richardson and G. C. Wood, "A Study of the Pitting Corrosion of Al by Scanning Electron Microscopy," Corros. Sci. 10, 313-323 (1970).
4. G. C. Wood, W. H. Sutton, J. A. Richardson, T. N. K. Riley, and A. G. Malherbe, "The Mechanism of Pitting of Aluminum and Its Alloys," pp. 526-546 in Localized Corrosion, Nat'l Assoc. Corros. Eng., 1974.
5. F. D. Bogar and R. T. Foley, "The Influence of Chloride Ion on the Pitting of Aluminum," J. Electrochem Soc. 119, 462 (1972).
6. W. K. Johnson, "Recent Developments in Pitting Corrosion of Aluminum," Br. Corros. J. 6, 200 (1971).
7. M. J. Pryor, "Electrode Reactions on Oxide Covered Aluminum," Z. Electrochem 62, 782 (1958).
8. M. A. Heine, D. S. Keir, and M. J. Pryor, "The Specific Effects of Chloride and Sulfate Ions on Oxide-Covered Aluminum," J. Electrochem. Soc. 112, 24 (1965).
9. H. Bohni and H. H. Uhlig, "Environmental Factors Affecting the Critical Pitting Potential of Aluminum," J. Electrochem. Soc. 116, 906 (1969).
10. J. R. Gavele, "Transport Processes and the Mechanism of Pitting of Metals," J. Electrochem. Soc. 123, 464 (1976).
11. M. J. Pryor, "The Influence of the Defect Structure of Aluminum Oxide Films on the Pitting of Aluminum Chloride Solutions," pp. 2-11, in Localized Corrosion, Nat'l Assoc. Corros. Eng., 1974.

TABLE I: NOMINAL COMPOSITIONS OF ALUMINUM ALLOYS

<u>Alloy</u>	<u>G*</u>	<u>R**</u>	<u>K***</u>
Hg	0.047%	0.03-0.06%	--
Zn	0.45%	1.25-2.0%	6.0-7.4%
Cu	0.019%	0.003% max	0.005% max
Fe	0.034%	0.007% max	0.10% max
Sn	--	--	0.12-0.20%
Si	--	--	0.10% max

*Alloy G: Galvalum[®] I (Dow Chemical USA)

**Alloy R: Reynode[®] II (Reynolds Metal Company)

***Alloy K: KA-90[®] (Kaiser Magnesium Company)

LIST OF FIGURES

- Figure 1: Macroscopic dissolution behavior of the aluminum anodic samples in synthetic seawater. Alloy G initiates attack which spreads laterally inward from the specimen edges. Alloy R forms elongated cavities on the broad faces of the specimen. Alloy K forms more (and smaller) dissolution sites per unit surface area.
- Figure 2: Microscopic dissolution morphology found within the dissolution regions of the respective alloys. Alloy G displays a distinct step pattern on all grain surfaces, whereas Alloy R forms surfaces usually made up of sharp peaks; both Alloy G and R accumulate little corrosion product on the dissolution surface. If the corrosion product is removed from Alloy K, a less distinct step structure is seen, with intergranular penetration.
- Figure 3: Microscopic observations of true (occluded cell) pitting phenomena observed within the dissolution regions of Alloys G and K when these regions become somewhat filmed over (after several days exposure). Alloys G and K develop mounds with smooth hemispherical caps that emerge from the pit mouths within a cracked film. Alloy K develops inflated pod-like domes in the general film on the unattacked regions of the anode.
- Figure 4: Less frequently observed are pitting and mound features on the unattacked regions of alloys G and R.
- Figure 5: Broken hemispherical pod on Alloy K; note the interior filament of corrosion product emerging from the pit mouth.

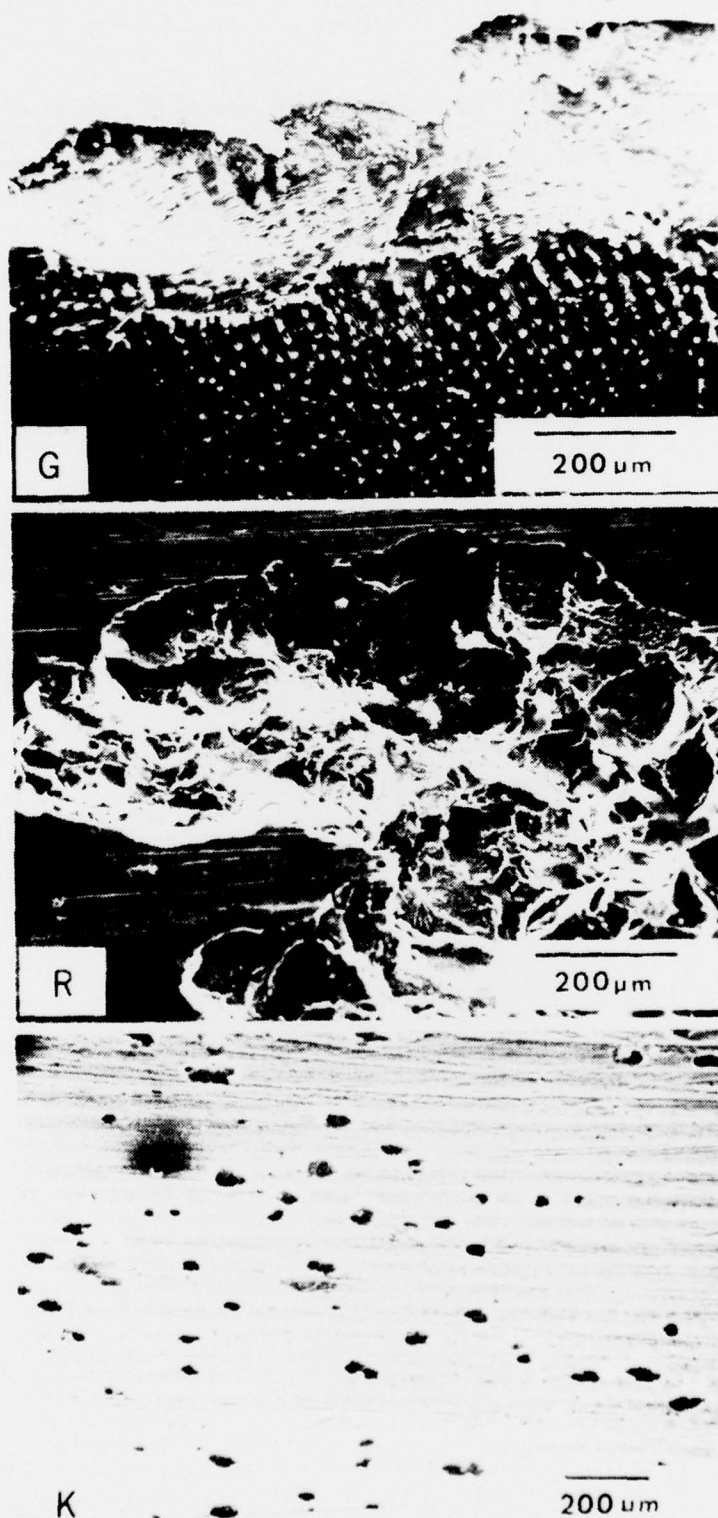


Figure 1: Macroscopic dissolution behavior of the aluminum anodic samples in synthetic seawater. Alloy G initiates attack which spreads laterally inward from the specimen edges. Alloy R forms elongated cavities on the broad faces of the specimen. Alloy K forms more (and smaller) dissolution sites per unit surface area.

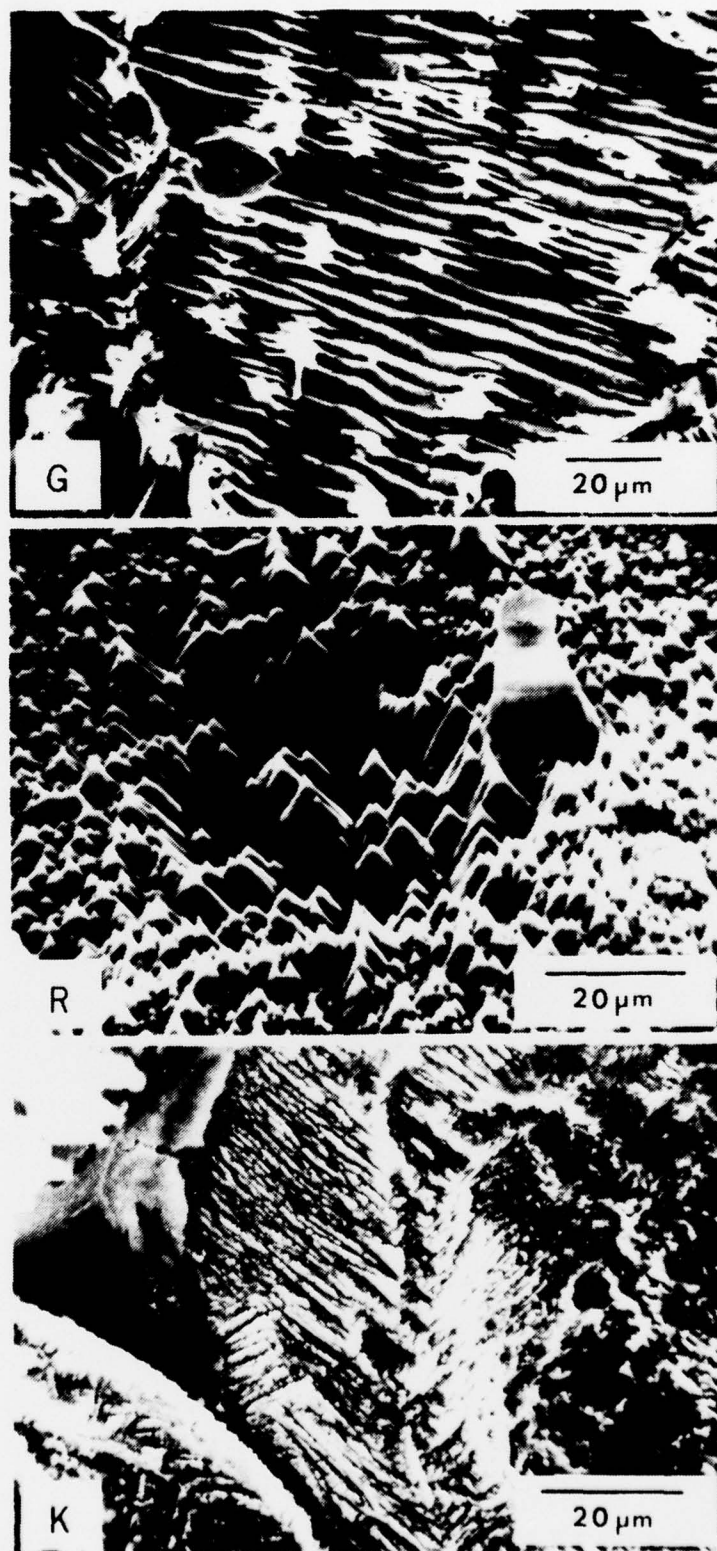


Figure 2: Microscopic dissolution morphology found within the dissolution regions of the respective alloys. Alloy G displays a distinct step pattern on all grain surfaces, whereas Alloy R forms surfaces usually made up of sharp peaks; both Alloy G and R accumulate little corrosion product on the dissolution surface. If the corrosion product is removed from Alloy K, a less distinct step structure is seen, with intergranular penetration.

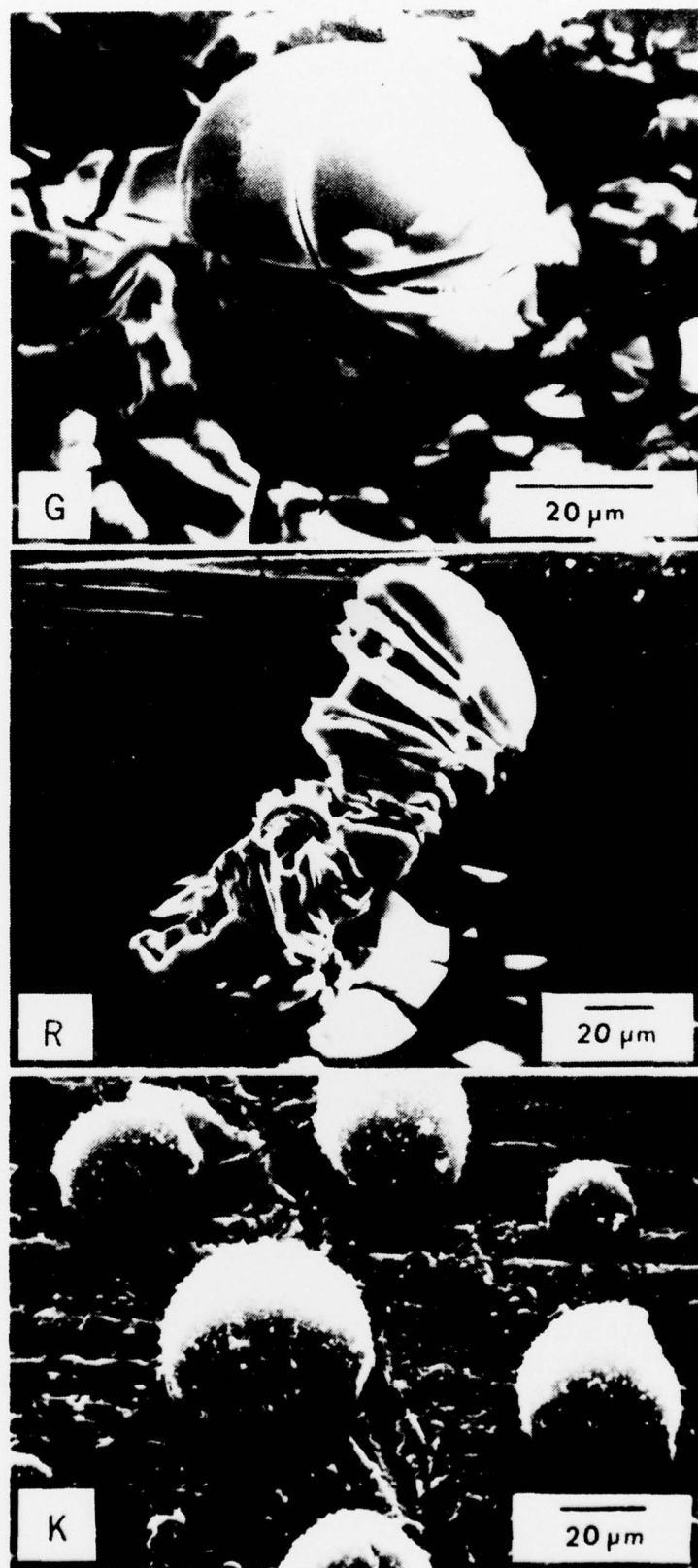


Figure 3: Microscopic observations of true (occluded cell) pitting phenomena observed within the dissolution regions of Alloys G and K when these regions become somewhat filmed over (after several days exposure). Alloys G and K develop mounds with smooth hemispherical caps that emerge from the pit mouths within a cracked film. Alloy K develops inflated pod-like domes in the general film on the unattacked regions of the anode.

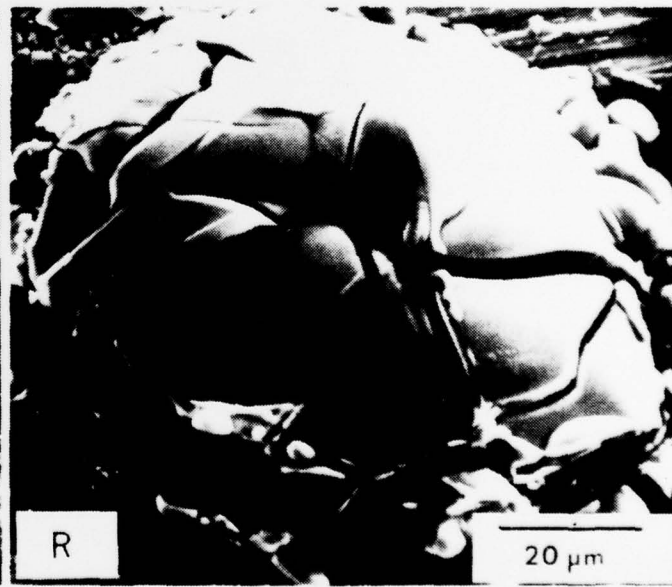
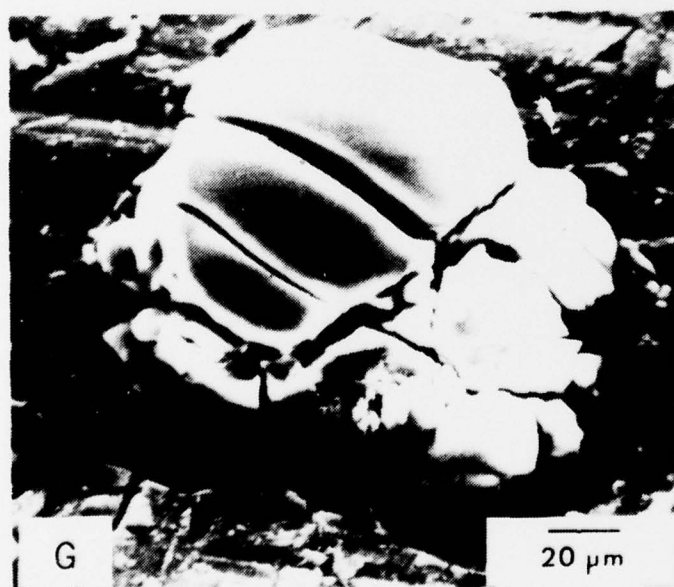
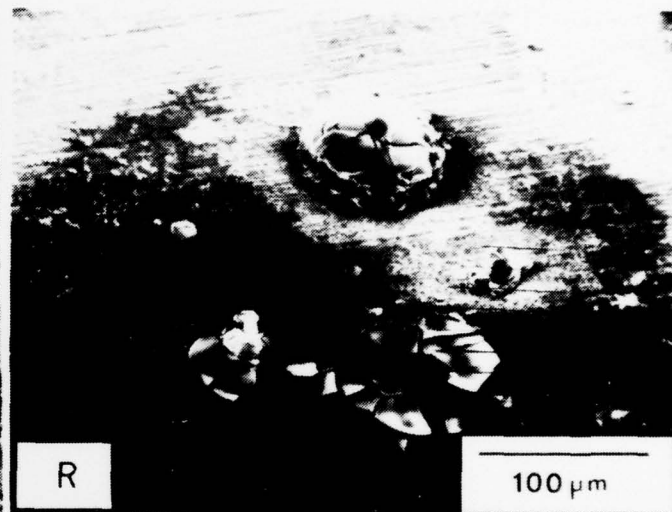
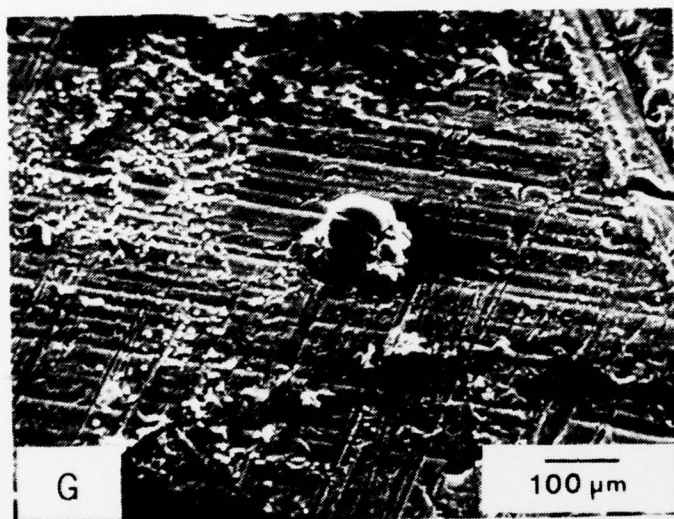


Figure 4: Less frequently observed are pitting and mound features on the unattacked regions of alloys G and R.

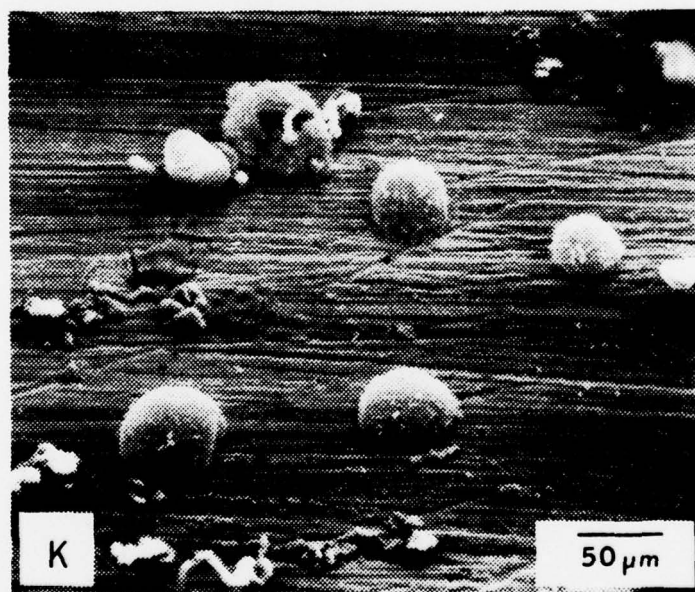


Figure 5: Broken hemispherical pod on Alloy K; note the interior filament of corrosion product emerging from the pit mouth.

INITIAL DISTRIBUTION LIST

	<u>No. Copies</u>
1. Defense Documentation Center Cameron Station Alexandria, Virginia 22314	2
2. Library, Code 0142 Naval Postgraduate School Monterey, California 93940	2
3. Department Chairman, Code 69 Department of Mechanical Engineering Naval Postgraduate School Monterey, California 93940	2
4. Naval Research Laboratory Washington, D. C. 20390 Code 2627	1
5. Naval Air Propulsion Test Center Trenton, NJ 08628 Attn: Library	1
6. Office of Naval Research Department of the Navy (Attn: Code 471) 800 N. Quincy Street Arlington, VA 22217	1
7. Naval Air Development Center Code 302 Warminster, PA 18974 Attn: Mr. F. S. Williams	1
8. Naval Construction Battalion Civil Engineering Laboratory Port Hueneme, CA 93043 Attn: Materials Division	1
9. Office of Naval Research 800 N. Quincy Street Arlington, VA 22217 Attn: Code 102	1
10. Naval Electronics Lab. Center San Diego, CA 92152 Attn: Electron Materials Sciences Division	1
11. Naval Missile Center Materials Consultant Code 3312-1 Point Mugu, CA 93041	1

- | | | |
|-----|---|---|
| 12. | Office of Naval Research
800 N. Quincy Street
Arlington, VA 22217
Attn: Code 470 | 1 |
| 13. | Commanding Officer
Naval Surface Weapons Center
White Oak Laboratory
Silver Spring, MD 20910 | 1 |
| 14. | David W. Taylor
Naval Ship R & D Center
Materials Department
Annapolis, MD 21402 | 1 |
| 15. | Commanding Officer
Office of Naval Research
Branch Office
495 Summer Street
Boston, MA 02210 | 1 |
| 16. | Naval Undersea Center
San Diego, CA 92132
Attn: Library | 1 |
| 17. | Naval Underwater System Center
Newport, RI 02840
Attn: Library | 1 |
| 18. | Commanding Officer
Office of Naval Research
Branch Office
536 S. Clark Street
Chicago, IL 60605 | 1 |
| 19. | Naval Weapons Center
China Lake, CA 93555
Attn: Library | 1 |
| 20. | Naval Air Systems Command
Washington, D. C. 20360
Attn: Code 52031 | 1 |
| 21. | Office of Naval Research
San Francisco Area Office
760 Market Street, Rm 447
San Francisco, CA 94102 | 1 |
| 22. | Naval Air Systems Command
Washington, D. C.
Attn: Code 52032 | 1 |
| 23. | Naval Air Systems Command
Washington, D. C. 20360
Attn: Code 320 | 1 |

- | | | |
|-----|--|---|
| 24. | Naval Research Lab.
Washington, DC 20390
Attn: Code 6000 | 1 |
| 25. | Naval Sea System Command
Washington, DC 20362
Attn: Code 035 | 1 |
| 26. | NASA Headquarters
Washington, D. C.
Attn: Code RRM | 1 |
| 27. | Naval Research Lab.
Washington, DC 20390
Attn: Code 6100 | 1 |
| 28. | Naval Facilities
Engineering Command
Alexandria, VA 22331
Attn: Code 03 | 1 |
| 29. | NASA
Lewis Research Center
20111 Brookpark Road
Cleveland, Ohio 44135
Attn: Library | 1 |
| 30. | Naval Research Lab.
Washington, D.C. 20390
Attn: Code 6300 | 1 |
| 31. | Scientific Advisor
Commandant of the Marine Corps
Washington, D. C. 20380
Code AX | 1 |
| 32. | National Bureau of Standards
Washington, DC 20234
Attn: Metallurgy Division
Inorganic Mat. Div. | 1 |
| 33. | Dr. Wm. R. Prindle
National Academy of Sciences
National Research Council
2101 Constitution Ave.
Washington, DC20418 | 1 |
| 34. | Dr. R. P. Wei, Lehigh Univ.
Inst. for Fracture &
Solid Mechanics
Bethlehem, PA 18015 | 1 |
| 35. | Prof. H. G. F. Wilsdorf
Univ. of Virginia
Dept. of Mat. Science
Charlottesville, VA 22903 | 1 |

36. Defense Metals and Ceramics 1
Info Center
Battelle Mem. Institute
505 King Ave.
Columbus, Ohio 43201
37. Naval Ship Engr. Center 1
CTR BG #2 Code 6101
3700 E-W Highway
Prince George Plaza
Hyattsville, MD 20782
38. Director, Ordnance Research Lab. 1
P.O. Box 30
State College, PA 16801
39. Army Research Office 1
Box CM, Duke Station
Durham, NC 27706
Attn: Metallurgy & Cer. Div.
40. Army Materials and Mechanics 1
Research Center
Watertown, MA 02172
Attn: (AMXMR-P)
41. Dir. Applied Physics Lab. 1
University of Washington
1013 NE 40th Street
Seattle, WA 98105
42. Metals and Ceramics Div. 1
Oak Ridge Nat'l Lab.
P.O. Box X
Oak Ridge, TN 37380
43. AF/Ofc. of Scientific Research 1
Bldg. 410 Bolling AF Base
Washington, D. C. 20332
Attn: Chem. Sci. Directorate
Electronics & S. S. Sci. Director
44. Los Alamos Scientific Lab 1
P.O. Box 1663
Los Alamos, NM 87544
Attn: Report Librarian
45. AF Materials Lab. (LA) 1
Wright-Patterson AFB
Dayton, Ohio 45433
46. Argonne National Lab. 1
Metallurgy Division
P.O. Box 229
Lemont, IL 60439

47. Dr. J. A. S. Green 1
Martin Marietta Corp.
1450 S. Rolling Road
Baltimore, MD 21227
48. Dr. T. R. Beck ;
Electrochemical Tech. Corp.
10035 31st Ave. NE
Seattle, WA 98125
49. Prof. R. H. Heidersbach 1
University of Rhode Island
Department of Ocean Engr.
Kingston, RI 02881
50. Professor I. M. Bernstein ;
Carnegie-Mellon Univ.
Schenley Park
Pittsburgh, PA 15213
51. Professor H. K. Birnbaum 1
Univ. of Illinois
Dept. of Metallurgy
Urbana, IL 61801
52. Prof. J. P. Hirth 1
Ohio State University
Metallurgical Engineering
Columbus, OH 43210
53. Prof. H. Herman 1
State Univ. of New York
Materials Science Div.
Stony Brook, NY 11794
54. Dr. Otto Buck 1
Rockwell International
1049 Camino Dos Rios
P.O. Box 1085
Thousand Oaks, CA 91360
55. Dr. D. W. Hoepfner 1
University of Missouri
College of Engineering
Columbia, MO 65201
56. Prof. H. W. Pickering 1
Pennsylvania State Univ.
Dept. of Mat. Sciences
University Park, PA 16802
57. Dr. David L. Davidson 1
Southwest Research Inst.
8500 Culebra Road
P.O. Drawer 28510
San Antonio, TX 78284

58. Dr. E. W. Johnson 1
Westinghouse Electric Corp.
Research and Development Center
1310 Beulah Road
Pittsburgh, PA 15235
59. Dr. F. Mansfeld 1
Rockwell
1049 Camino Dos Rios
P.O. Box 1085
Thousand Oaks, CA 91360
60. Dr. D. J. Duquette 1
Dept. of Metallurgical Engr.
Rensselaer Polytechnic Inst.
Troy, NY 12181
61. Prof. R. T. Foley 1
The American University
Dept. of Chemistry
Washington, DC 20016
62. Prof. A. E. Miller 1
University of Notre Dame
College of Engineering
Notre Dame, IN 46556
63. Mr. G. A. Gehring 1
Ocean City Research Corp.
Tennessee Ave. & Beach Thorofare
Ocean City, NJ 08226
64. Prof. R. W. Staehle 1
Ohio State University
Dept. of Metallurgical Engr.
Columbus, OH 43210
65. Dr. Barry C. Syrett 1
Stanford Research Institute
333 Ravenswood Avenue
Menlo Park, CA 94025
66. Brookhaven Nat'l Laboratory 1
Technical Info. Div.
Upton, LI
New York 11973
Attn: Research Library
67. Library 1
Building 50 Rm 134
Lawrence Radiation Laboratory
Berkeley, CA 94550
68. Prof. Jeff Perkins 30
Naval Postgraduate School
Code (69Ps)
Monterey, CA 93940